Mechanosensitivity of Membrane Budding and Trafficking

Lionel Foret

Abstract Intracellular compartments continually exchange material transported by small vesicles or tubules, which are formed in the membrane of the donor compartments and eventually fuse with the membrane of the receptor compartments. The formation and fission of a membrane bud giving rise to a new object and the fusion are controlled to some extent by the mechanical properties of the membranes, in particular their tension. In this chapter, we review the different mechanisms of vesicle and tubule budding and analyze the influence of the membrane tension on these processes using basic considerations of thermodynamics and mechanics. In any case, vesicle and tubule production can be impaired at high enough tension. Next, we discuss the influence of tension on membrane fusion, which is a less understood problem. Finally, since the release/absorption of vesicles or tubules should affect the tension of the donor/receptor, we speculate about the possible regulatory role of the membrane tension on intracellular trafficking and compartments stability.

Keywords Intracellular trafficking · Biological membrane · Budding · Fusion · Tension

1 Introduction

Eukaryotic cells comprise several intracellular compartments, also named organelles, bound by a fluid membrane made of lipids and proteins. The biochemical composition of the membrane defines the nature and the functions of the compartment. Examples of organelles are the endoplasmic reticulum, the Golgi apparatus, the different types of endosomes, and the lysosomes. These compartments continually exchange material with each other and with the plasma

L. Foret (✉)
Ecole Normale Supérieure, CNRS, UPMC Univ Paris 06, Laboratoire de Physique Statistique, Paris, France
e-mail: lforet@lps.ens.fr

membrane. The material is carried from one compartment to another by very small membrane-bound objects: transport vesicles and tubules. The genesis of a transport vesicle or tubule takes place in the membrane of the donor compartment. A local membrane deformation emerges, a process called "budding," and eventually undergoes fission giving rise to a new membrane-bound object. The vesicle or tubule released by this mean moves in the cell, pulled by molecular motors along filaments, and eventually fuses with the membrane of the target compartment where the transported material should be delivered [2, 6, 9]. All these processes, such as budding, fission, motion, and fusion are mediated by energy consuming protein machineries. The diameter of transport vesicles is of the order of 100 nm or smaller. Tubules diameter is of the order of few tens of nm and their length up to several hundred nm.

Membrane budding, fission, and fusion involve significant modifications of the membrane shape. These processes should thus be sensitive on the mechanical properties of the membrane. Depending on the membrane elasticity and tension, budding, fusion, and fission can be either facilitated or prevented. The morphology of the budding structures and released objects depends also on the mechanical parameters characterizing the donor membrane. Living cells might use this mechanosensitivity to mechanically regulate the intracellular traffic.

For large-scale deformations with respect to membrane thickness, a membrane can be described as an unstretchable bi-dimensional fluid, which elastically opposes bending [85]. The elastic modulus, or bending rigidity κ, of a biological membrane is of the order of 10^{-19} J. The membranes of the cell and of the intracellular compartments are under tension, with σ of the order of 10^{-5} N/m. This parameter in particular can play an important role in traffic regulation by its influence on budding and fusion processes.

The outline of this chapter is as follows. Section 2 presents some generality on the membrane budding process. Sections 3 and 4 are devoted to the mechanics of vesicle budding and tubule budding, respectively. The two main questions that are addressed are "how tension and rigidity affects the shape of the budding protrusions" and "under which conditions on tension and rigidity is budding possible." The theoretical predictions are compared with experimental observations. In particular, in vitro experiments on reconstituted systems, in which the mechanical parameters can be measured and sometime tuned, have provided much insights on these questions. In Sect. 5, the influence of the membrane tension on fusion is discussed. The first question that is addressed is the dependence of the fusion barrier on the tension. Despite the insights provided by molecular simulations this last decade, this question remains not well understood. The second question is the effect of tension gradient for the transport between fusing objects. Section 6 is a more speculative discussion on the possible regulatory role of membrane tension on intracellular trafficking. Tension affects budding, fission, and fusion but on the other hand, all these processes can potentially affect compartments tension by adding and removing membrane area. This mutual interaction could allow to coordinate the entry and secretion of vesicles and tubules in a compartment.

2 Membrane Budding: Generality

The first step in the genesis of a tubule or a vesicle is the gradual deformation of an initially nearly flat membrane. This is the budding process that precedes the eventual fission of the narrow membrane tubes that connects the vesicular or tubular protrusion to the rest of the membrane. The rigidity of the membrane against bending and the membrane tension oppose to membrane deformation and thus oppose to budding. Using the thin elastic fluid membrane model, the free energy of a membrane is

$$\mathcal{F}_{m} = \int_{A} \left[\frac{\kappa}{2} \left(C_1 + C_2 - C_0 \right)^2 + \kappa_G C_1 C_2 + \sigma \right] dA \tag{1}$$

where A is the membrane area, C_1 and C_2 are the principal local curvatures, κ the bending rigidity, κ_G the Gaussian bending rigidity, σ the tension, and C_0 the spontaneous curvature. The integral over the Gaussian curvature $C_1 C_2$ is constant in budding processes [90]. The Gaussian bending rigidity κ_G thus plays no role in membrane budding and this term is omitted in the following. The energetic cost associated with the formation of a vesicle is roughly, $\mathcal{F}_m = 8\pi\kappa + 4\pi R^2 \sigma \sim 1000 \, k_B T$ for a vesicle radius $R = 50$ nm. Therefore, budding cannot occur spontaneously. It requires the action of proteins able to shape the membrane. A short review of the different mechanisms used by the cell to bend membrane and generate transport carriers is provided in the following Sect. 2.1. Whether vesicle or tubule can or cannot bud from a flat membrane, and the morphology of the budding structure, results from the competition between, on one hand the action of the proteins inducing membrane deformation, and on the other hand the membrane tension and rigidity, which oppose deformation. This issue is addressed in Sects. 3 and 4, in the case of vesicle and tubule, respectively, using simple mechanical and thermodynamical considerations. Section 2.2 presents the basics of elasticity for axisymmetrical membrane that are used to compute membrane bud shape and energy.

2.1 Mechanisms of Membrane Curvature Generation

Several reviews on this topic have been written, see [46, 52, 69, 93, 101, 125]. Here, only a brief overview of the different mechanisms is given.

- **Rigid coat formation**. Specialized peripheral proteins polymerize to form a rigid structure, which imposes its own curved shape to the membrane on which it adheres. The word coat is usually restricted to spherical protein assembly responsible for vesicle budding. Here we shall use it in a more general way, including rigid tubular structures formed by Dynamin or F-BAR proteins, for example.

- **Protein crowding**. The lateral pressure arising from the steric repulsion between peripheral proteins bound on one side of the membrane promotes membrane bending. Curvature increases the area accessible to the proteins, which is entropically favorable [99, 100].
- **Curved shape proteins**. Peripheral proteins with a curved membrane-binding side, such as those with a BAR (Bin-Amphiphysin-Rvs) domain [34], impose locally their curved shape, driving membrane deformation. Integral proteins with an asymmetrical shape should behave in an analogous way.
- **Wedge effect**. Peripheral proteins with amphipathic helices, such as ENTH (Epsin N-Terminal Homology) domain, or loop, inserted in the lipid bilayer act as wedge able to locally bend the membrane [10, 54].
- **External force**. Membrane deformation can also be driven by normal forces produced by actin filaments and molecular motors pushing or pulling the membrane [58].
- **Lipid asymmetry**. Finally, curvature can be induced by composition asymmetry between the two lipid layers, generated and maintained by enzymes that modify lipid tail or head [69, 125].

## 2.2 Elasticity of Axisymmetrical Membrane

Vesicle or tubule budding driven by protein machineries is a slow process (typically few tens of second for spherical coat assembling) as compared to membrane shape relaxation. The membrane is always at mechanical equilibrium and its shape minimizes the energy (1).

Tubular and vesicular are axisymmetrical structures. The membrane shape can be parametrized by the cylindrical coordinates $r(s)$ and $z(s)$, where s is the arc length along the shape contour, and by the angle $\psi(s)$, Fig. 1. These three quantities are not independent but obey,

$$\dot{r} = \cos \psi \, , \quad \dot{z} = - \sin \psi \, , \tag{2}$$

where the dot denotes the derivative with respect to s. The two principal curvatures of the membrane are $C_1 = \dot{\psi}$ and $C_2 = \sin \psi / r$, and the area differential

Fig. 1 Shape parametrization for an axisymmetric membrane. The red line is the contour of the membrane shape
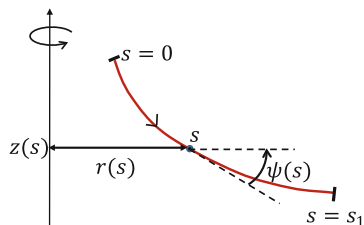
$dA = 2\pi r ds$. The membrane free energy (1) then reads,

$$\mathcal{F}_{\mathrm{m}} = 2\pi \int_0^{s_1} \left[\frac{\kappa}{2} \left(\dot{\psi} + \frac{\sin \psi}{r} - C_0 \right)^2 + \sigma \right] r \, ds \; . \tag{3}$$

The equations satisfied by $r(s)$, $z(s)$, and $\psi(s)$ at equilibrium are obtained by minimizing (3). Inserting the equilibrium $r(s)$, $z(s)$, and $\psi(s)$ in (3) then gives the energy of the membrane deformation. The minimization procedure is detailed in [49, 90] and summarized in Appendix 1. Accounting for the possible pressure difference p across the membrane and punctual normal force f applied at the membrane center $r = 0$, the equation derived from energy minimization reads,

$$\ddot{\psi} \cos \psi + \frac{\dot{\psi} \cos^2 \psi}{r} + \frac{\dot{\psi}^2 \sin \psi}{2} - \frac{\sin \psi}{2r^2} \left(2 \cos^2 \psi + (\sin \psi - C_0 r)^2 \right)$$
$$- \frac{\sigma}{\kappa} \sin \psi + \frac{p}{2\kappa} r + \frac{f}{2\pi \kappa r} = 0 \; , \tag{4}$$

which together with Eq. (2) form a complete set of equations satisfied by $r(s)$, $z(s)$, and $\psi(s)$ at equilibrium.

3   Vesicle Budding Driven by Rigid Coat Assembling

In living cell, rigid coat assembling on membrane is the main mechanism driving vesicle budding. Various proteins polymerize on the membrane, forming a rigid shell, or "coat," with spherical cap shape that covers the membrane. The coat grows until the formation of a nearly complete sphere [51]. The three main types of coat, clathrin coat [68], COPI [5, 44], and COPII [122] are made of different components and assemble on the membrane of different organelles (plasma membrane and endosome, Golgi apparatus, endoplasmic reticulum, respectively) but they share strong similarities regarding their structure and function [24, 70]. Coat assembling is passive, only driven by the free energy gain associated with components polymerization, and can be reconstituted in vitro with minimal sets of proteins. Vesicle formation results from the competition between the energy gain due to coat polymerization and the cost due to membrane deformation.

In the simplest model, a protein coat is a continuous spherical cap with curvature radius R. The degree of completion is characterized either by the angle $0 \leq \alpha \leq \pi$ defined on Fig. 2, or by the ratio $0 \leq x \leq 1$ of the coat area to the complete sphere area,

$$x = \frac{A_{\mathrm{c}}}{4\pi R^2} = \frac{1}{2}(1 - \cos \alpha), \tag{5}$$

Fig. 2 The spherical cap model. The blue line is the membrane area covered by a coat. The red line is the membrane neck
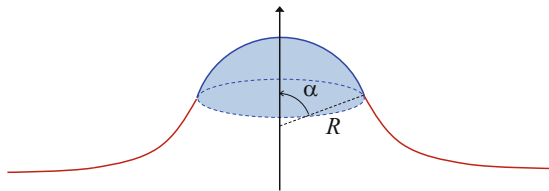
A coat imposes its spherical cap shape on the membrane in the area where it adheres. The deformation propagates around the coat in a region that we call membrane *neck*, Fig. 2.

The spherical cap assumption for the coat shape is used in the following to study theoretically the shape of the membrane neck (Sect. 3.1) and its energy (Sect. 3.2) at different stages of vesicle budding and for different tension and rigidity. Then, using energetic considerations, the conditions required for vesicle budding to occur are analyzed in Sects. 3.3 and 3.4.

3.1 Shape of the Membrane Neck

The shape of the membrane around the coat might play an important role in the coordination of the budding and fission machinery [3, 84]. Several proteins involved in vesicle formation are curvature sensor, they bind and concentrate preferentially in regions with particular curvature [74, 98].

Under the spherical cap approximation, the neck is axisymmetric and its shape can be calculated using Eqs. (2), (4). We assume that the pressure difference across the membrane, the spontaneous curvature of the membrane, and the pulling force are zero ($C_0 = p = f = 0$). The deformation is imposed by the rigid coat through the boundary conditions. Equations (2), (4) contain a single parameter, the length

$$\lambda = \sqrt{\frac{\kappa}{\sigma}} \, , \tag{6}$$

which sets the typical extension of the membrane deformation around the coat. At the coat boundary, the radius and the angle are fixed and depend on the completion level of the coat, $r(0) = R \sin \alpha$ and $\psi(0) = \alpha$. Far from the coat, the membrane should recover its planar shape, $\psi(\infty) = \dot{\psi}(\infty) = z(\infty) = 0$. The shape of the membrane neck then depends on two dimensionless parameters: α and $(R \sin \alpha)/\lambda$.

Figure 3 shows the membrane contour, computed numerically, at different stages of the coat growth, i.e., for different values of α, and for different values of R/λ. The morphology strongly depends on the tension. At high tension, the deformation is concentrated in a very narrow and highly curved region near the coat. At low tension, the curvature is low and the deformation propagates far from the coat. Approximate analytical expressions for the membrane shape can be derived in different limit cases [28].
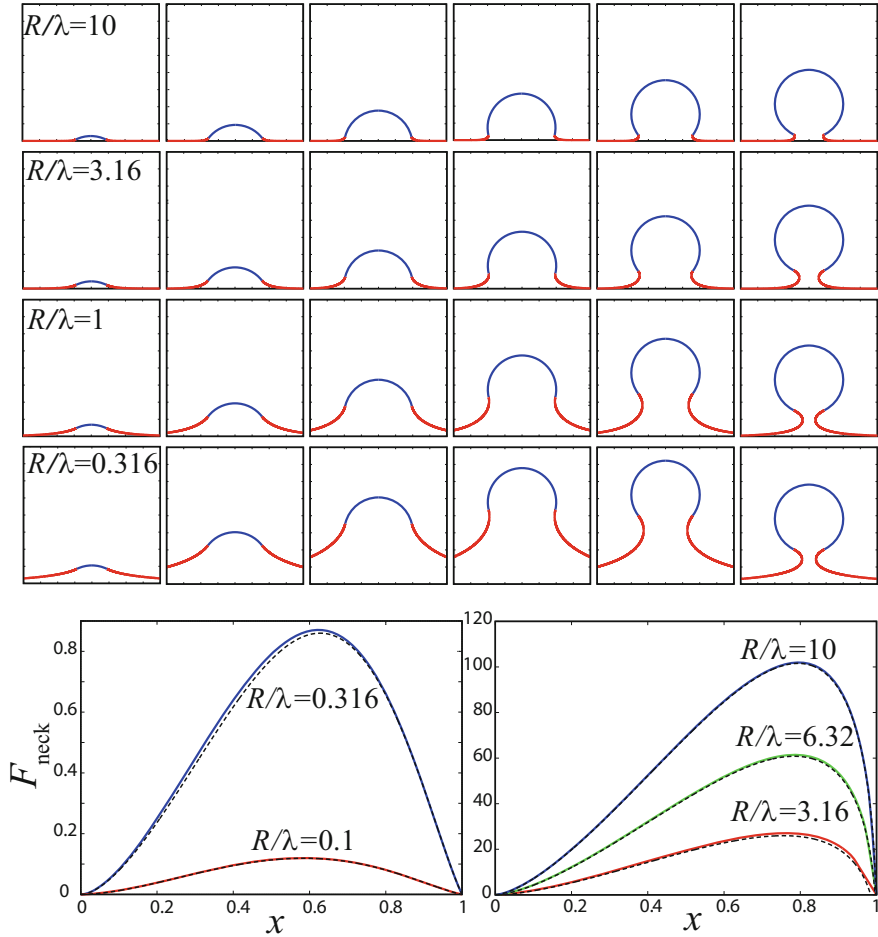
Fig. 3 Top panels: shape of the membrane neck during coat growth, i.e., for different values of α: $0.15\pi, 0.28\pi, 0.42\pi, 0.57\pi, 0.71\pi, 0.85\pi$ from the left to the right, and different values of $R/\lambda = R\sqrt{\sigma/\kappa}$, see the values on the graph. The unit length in the graphs is $\lambda/2$. Bottom panels: energy of the membrane neck $\mathcal{F}_{\text{neck}}$ outside the coat as a function of x, the coat completion parameter, for different values of R/λ (see graph). The dash black line corresponds to the approximations, Eq. (16), in the low tension limit (left) and large tension limit (right)

3.1.1 Weak Deformation

When α is small, or far from the coat, the membrane deformation is weak, $\psi \ll 1$. In this limit, the shape equations (4), (2) can be linearized,

$$\ddot{\psi}r^2 + \dot{\psi}r - (1 + (\sigma/\kappa)r^2)\psi = 0, \quad \dot{r} = 1, \quad \dot{z} = -\psi \qquad (7)$$

and solved analytically,

$$r = s + a, \quad \psi = \beta K_1(r/\lambda), \quad z = \beta \lambda K_0(r/\lambda) . \tag{8}$$

The Bessel functions K_0 and K_1 decrease exponentially at $s \gg \lambda$. The tension imposes a flat shape at a distance larger than λ. When α is small, the integration constants a and β are given by the boundary conditions at the coat border, $a = R \sin \alpha$ and $\beta = \alpha / K_1(R \sin \alpha / \lambda)$; when α is not small, the solution of the linearized equation is valid only at large enough distance from the coat, a and β depend on the shape near the coat.

3.1.2 Low Tension or Near Full Completion

In the limit $R \sin \alpha \ll \lambda$, the tension has a negligible effect near the coat at $r \ll \lambda$. At zero tension, the free energy (1) is minimum when the mean curvature is zero at each point of the membrane, $C_1 + C_2 = 0$ or using Eq. (3),

$$\dot{\psi} + \frac{\sin \psi}{r} = 0 . \tag{9}$$

The solution of this equation combined with Eq. (2) is the catenoid,

$$r = \sqrt{(s - s_0)^2 + r_0^2}, \quad \psi = \arcsin (\pm r_0/r) , \quad z = \mp r_0 \operatorname{arcosh}(r_0/r) + z_0 ,$$

with $s_0 = R \cos \alpha \sin \alpha$ and $r_0 = R \sin^2 \alpha$. $\tag{10}$

The sign in the second equation (resp. third equation) is $+$ if $s > s_0$ (resp. $-$), and reciprocally if $s < s_0$. The integration constants s_0 and r_0 are determined using the boundary conditions; r_0 is the neck radius at the narrowest position when $\alpha > \pi/2$. The principal curvatures are in general $C_1 = -C_2 = r_0/r^2$ and take their maximum absolute value $1/r_0$ where the neck is the narrowest.

Equation (10) provides a good approximation of the membrane shape near the coat, for $r \ll \lambda$. On the other hand, at large distance from the coat, the deformation is weak and the shape obeys (8). According to (10), the weak deformation condition holds for $r \ll r_0$. Thus, the ranges of validity of the two approximations, weak deformation at $r \gg r_0$ and catenoid at $r \ll \lambda$, overlap. Matching the two approximations gives the integration constants: $\beta = r_0/\lambda$ in (8) and, $z_0/r_0 = -\gamma_e + \ln(4\lambda/r_0)$ in (10) with $\gamma_e \simeq 5.77$ the Euler constant.

3.1.3 Large Tension

In the limit $(R/\lambda) \sin \alpha \gg 1$, the deformation is localized close to the coat boundary, in a region of width λ much thinner than the radius of the coat border $R \sin \alpha$. The

curvature of the coat periphery has a negligible influence on the membrane shape. Keeping only the higher order terms in r, Eq. (4) reduces to,

$$\ddot{\psi} \cos \psi + \frac{\dot{\psi}}{2} \sin \psi - \frac{\sigma}{\kappa} \sin \psi = 0 . \tag{11}$$

Integrating this equation gives $\dot{\psi} = -2\sqrt{\sigma/\kappa} \sin(\psi/2)$ and then,

$$\psi = 4 \arctan \left[\exp \left(\frac{s_0 - s}{\lambda} \right) \right] ,$$

$$r = R \sin \alpha + s + 2\lambda \left[\cos \left(\frac{\alpha}{2} \right) - \tanh \left(\frac{s - s_0}{\lambda} \right) \right] ,$$

$$z = \frac{2\lambda}{\cosh \left(\frac{s-s_0}{\lambda} \right)} , \quad \text{with} \ s_0 = \lambda \ln(\tan(\alpha/4)) . \tag{12}$$

The second and third relations are obtained from Eq. (2) and s_0 is deduced from the boundary conditions. The membrane curvature $C_1 = \dot{\psi}$ ($C_2 \ll C_1$) is maximum (in absolute value) at the coat boundary, $C_1 = (\sin \alpha/2)/\lambda$.

3.2 Energy of the Membrane Bud

The membrane energy associated with the formation of a single protrusion from a flat membrane is obtained by subtracting the energy of the flat membrane to the energy of the deformed membrane,

$$\mathcal{F}_{\text{bud}} = \mathcal{F}_{\text{m}} - \sigma A_0 , \tag{13}$$

where $\mathcal{F}_{\text{m}}$ is given by (1) and A_0 is the area of the initially flat membrane. The bud energy can be split into two contributions, the contribution from the membrane area under the coat and the contribution from the rest of the membrane (the neck),

$$\mathcal{F}_{\text{bud}} = \mathcal{F}_{\text{cap}} + \mathcal{F}_{\text{neck}} . \tag{14}$$

In the coat region, using the spherical cap approximation, the principal curvatures are $C_1 = C_2 = 1/R$. The spontaneous curvature of the membrane is assumed to be zero $C_0 = 0$. Characterizing the coat assembling state by x, the ratio of the cap area to the complete sphere (5), the cap area is $A = 4\pi R^2 x$ and $A_0 = \pi (R \sin \alpha^2) = 4\pi R^2 x (1 - x)$. The energy of the membrane bound to the coat is,

$$\mathcal{F}_{\text{cap}} = 8\pi \kappa x + 4\pi \sigma R^2 x^2 . \tag{15}$$

The energy of the neck is obtained by inserting the solution of the shape equations (4), (2) in the free energy (3) and by using $A_0 = 2\pi \int_0^{s_1} r \cos \psi$. Using the approximate expressions for the shape derived in the preceding section, one obtains (see [28] for detailed calculations),

$$\mathcal{F}_{\text{neck}} \simeq \begin{cases} 16\pi \sigma R^2 x^2 (1-x)^2 \left(-\gamma_e + \frac{x}{2(1-x)} - \ln \left(R\sqrt{\sigma/\kappa}\sqrt{x}(1-x)^{3/2} \right) \right) \\ 16\pi \sqrt{\kappa \sigma} R \sqrt{x(1-x)} \left(1 - \sqrt{1-x} \right) \\ \quad + 4\pi \kappa \left(x - 4 + 4\sqrt{1-x} - 2\ln \left(\frac{1+\sqrt{1-x}}{2} \right) \right). \end{cases}$$

(16)

The first line is the limit of low tension ($R \sin \alpha \ll \lambda$) with $\gamma_e \simeq 5.77$ the Euler constant, and the second line is the limit of large tension ($R \sin \alpha \gg \lambda$). Figure 3 shows the energy obtained numerically as a function of x in the large and low tension limits. It shows the good accuracy of the above approximate expressions.

3.3 Budding or Not Budding? Influence of the Tension and Rigidity

Vesicle budding is driven by the free energy gained by polymerizing proteins. The polymerization energy per unit of coat area μ accounts for protein–protein binding energy, for membrane–protein binding energy, and for the loss of entropy of the proteins initially dispersed in the cytosol. In the case of clathrin coat, the polymerization energy has been estimated to be $\sim 20\, k_B T$ per clathrin molecules or $\mu \sim 3\, k_B T / \text{nm}^2$ [19, 86]. For coat assembling to occur, the polymerization energy gain must counter-balance the cost associated with membrane deformation. Depending on the tension σ, the rigidity κ, and the polymerization energy μ, vesicle budding may or may not be possible.

The energy required to form a coat of spherical cap shape with the completion degree x reads,

$$\mathcal{F} = 4\pi \tau R \sqrt{x(1-x)} - 4\pi \mu R^2 x + \mathcal{F}_{\text{bud}}(x)$$

(17)

The last term $\mathcal{F}_{\text{bud}}$, the energy cost of the membrane deformation, is discussed in the preceding section. The second term is the energy gain due to coat polymerization $\mu \times A_c$. The first term accounts for the loss of binding energy of the coat components located at the coat edge. It is proportional to the line tension $\tau \sim k_B T/\text{nm}$ and to the coat perimeter $2\pi R \sin \alpha = 4\pi R \sqrt{x(1-x)}$.

Figure 4 shows a phase diagram obtained by minimizing the free energy (17). Depending on the value of $\sigma R^2/\kappa$ and $\mu R^2/\kappa$, the minimum is found at $x = 0$ (no coat assembling/no budding), or at $x = 1$ (complete vesicle budding), or at an intermediate value $0 < x^* < 1$ corresponding to a state where coat formation is
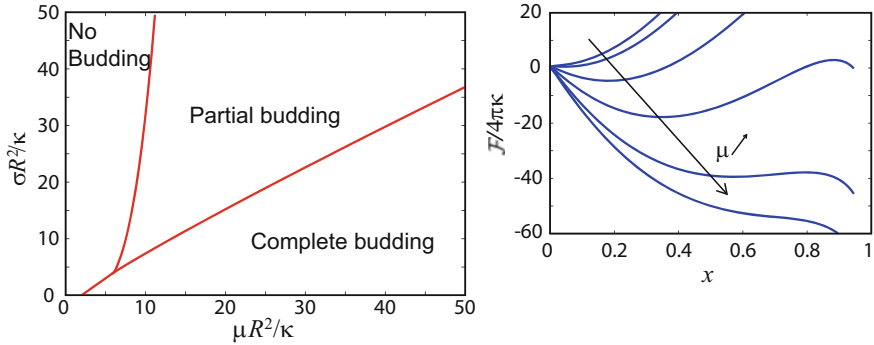
Fig. 4 Right: phase diagram obtained by minimizing $\mathcal{F}(x)$ given by (17). The minimum is either at $x = 0$ (no budding), $x = 1$ (complete budding), or $0 < x^* < 1$ (incomplete budding). Left: profile of $\mathcal{F}(x)$ for different values of μ at fixed $\sigma R^2/\kappa$ (in the large tension regime)

incomplete. The line separating the complete budding regime from the other regions of the phase diagram indicates the polymerization energy μ required to make a complete coat as a function of the tension.

At small tension, $\mathcal{F}_{\text{bud}} \simeq 8\pi\kappa x$ at the lowest order in $\sigma R^2/\kappa$. The function $\mathcal{F}(x)$ has a bell shape and the two minimum are at $x = 0$ and $x = 1$. The complete budding state $x = 1$ is the most energetically favorable if

$$\mu > \sigma + \frac{2\kappa}{R^2} \ . \tag{18}$$

At large tension, the energy landscape $\mathcal{F}(x)$ is shown in Fig. 4 for different values of μ. The membrane energy is approximately $\mathcal{F}_{\text{bud}} \simeq \sigma R^2 x^2$ at the lowest order in $\kappa/(\sigma R^2)$. The balance with the polymerization energy induces an energy well at

$$x^* \simeq \mu/2\sigma \ . \tag{19}$$

At large μ, the well disappears and the energy is minimum at $x = 1$. At small μ, the line tension prevents the appearance of the well, $\mathcal{F}(x)$ is monotonically increasing and is thus minimum at $x = 0$. The range where the intermediate minimum x^* exists is approximately,

$$(3/2)\tau^{2/3}\sigma^{1/3}R^{4/3} < \mu < 2\sigma \ . \tag{20}$$

The left side inequality is obtained by calculating the value of μ where the $\mathcal{F}(x)$ as an inflexion point using the approximation $\mathcal{F}_{\text{bud}} = \sigma R^2 x^2$ and $x \ll 1$. The right side inequality is deduced from the condition $x^* > 1$ using the approximation (19).

The main prediction of this simple model is that tension and rigidity can either prevent coat assembling, or arrest coat assembling in an incomplete state. How does it compare to experimental observations? In vitro reconstitution of COPI

coat assembling on liposomes, on GUV [64], and on lipid droplets [107, 108] demonstrates that budding is much favored at low tension and almost inhibited at large tension. On lipid droplets, the threshold tension was found to be $\simeq$ 2×10^{-3} N/m, which is located in the high tension regime of the phase diagram ($\sigma R^2/\kappa \simeq 900$ using $R = 60$ nm for COPI vesicles and $\kappa = 2\ k_B T$ for the monolayer bounding lipid droplets). Reconstitution of clathrin coat assembling on GUV [86] leads to similar results. Increasing tension and rigidity can impair clathrin assembling and even more striking, electron microscopy images showed the existence of stable shallow buds for an intermediate range of tension in agreement with theoretical predictions.

In living cell, the influence of tension on coat assembling has first been observed indirectly. Raucher and Sheetz [79] have shown strong correlation between the tension of the plasma membrane and the endocytosis rate, and thus indirectly on the rate of clathrin coated vesicle production. They suggested that tension could be an important regulator of endocytosis, its increase being responsible for the dramatic inhibition of endocytosis during mitosis. As a second example, a drug responsible for Golgi swelling, and presumably inducing the increase of its tension, is known to block COPI assembling, dramatically modifying the Golgi morphology [106].

More recently, Boulant et al. [7] have shown that actin is required for clathrin coated vesicle formation when the membrane tension is high. Disrupting actin polymerization, they observed that in membrane with high tension, clathrin coats remain arrested in an incomplete state, as predicted by the model. By pulling or pushing on the membrane bud, actin may provide the energy required to counter-balance the surface energy cost associated with coat growth. The force exerted by actin has been included in a continuous mechanical model of vesicle budding by Walani et al. [116]. They showed that this force applied to a partially coated bud leads to complete vesicle formation. The role of the tension in this actin-assisted budding case is also investigated.

Note finally that the spherical cap model studied in this section may also apply to caveola. Caveola are plasma membrane invaginations induced by oligomerization of caveolin proteins. Stretching the plasma membrane to increase the tension has been shown to lead to caveola disappearance [95].

3.4 Coat with Finite Rigidity

The vesicles produced by coat assembling can have different radius, allowing to incorporate cargo of different size [47, 68]. Clathrin coats can even form flat structures sometime named "plaques" [50]. One may wonder whether membrane tension or rigidity could influence the size and morphology of the coat. It has been proposed, for example, that high tension could lead to caveola flattening [91].

To address this issue, the spherical cap model can be generalized by assuming that the coat is an elastic layer with bending rigidity κ_c and preferential curvature radius R_c. For clathrin coat, the rigidity has been measured and is $\simeq 300\ k_B T$
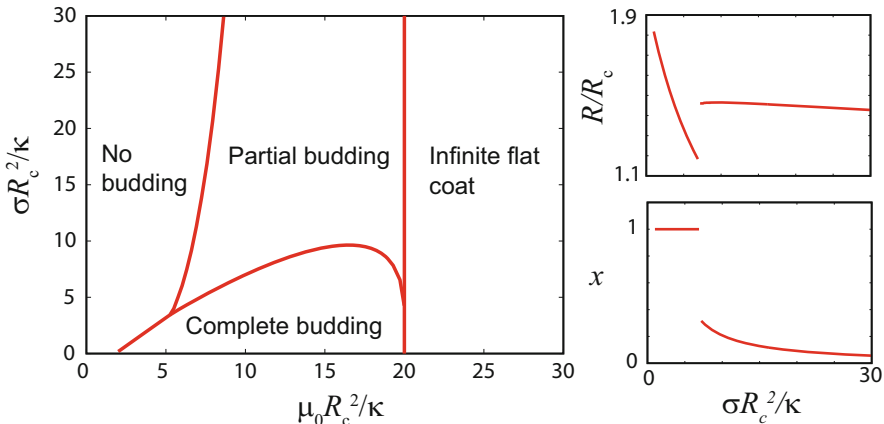
Fig. 5 Left: phase diagram for coat with finite rigidity $\kappa_c = 10\kappa$. Right: equilibrium value of R (top) and x (down) function of $\sigma R_c^2/\kappa$ for $\mu_0 R_c^2 \kappa = 10$

[48]. The morphology of the coat should then be calculated by solving the shape equation (4) in the coat and in the neck regions, as in [1, 116]. For simplicity here, let's assume that the coat shape is still a spherical cap with a radius R, which is now a free variable. The polymerization energy per area unit reads,

$$\mu(R) = \mu_0 - 2\kappa_c \left(\frac{1}{R_c} - \frac{1}{R} \right)^2 . \tag{21}$$

In a thermodynamic approach, the preferential state of a coat is obtained by minimizing $\mathcal{F}(x, R)$ (17), in which μ is given by (21), with respect to the two free variables x and R (or R and A_c, the coat area (5)). The new phase diagram is shown in Fig. 5. The three states $x = 1$, $x = 0$, and $0 < x < 1$ are still present. The most striking difference as compare to the case with infinite coat rigidity, shown in Fig. 4, is the vertical line delimiting a new state at high μ_0. In this region of the phase diagram, a coat assembles into a flat structure, which grows without bound. This prediction can be easily understood by considering the energy of a flat coat expressed as a function of the coat area A_c,

$$\mathcal{F} = \tau \sqrt{4\pi A_c} - (\mu_0 - 2\kappa_c/R_c^2)A_c . \tag{22}$$

It appears that if,

$$\mu_0 R_c^2 > 2\kappa_c , \tag{23}$$

a flat infinite coat is necessarily the energetically most favorable state. At the opposite, when this condition is not fulfilled, a flat coat cannot exist. Interestingly,

this analysis reveals that the transition toward the flat coat state is not controlled by tension.

The influence of the tension on the coat state is shown on the curves on the left of Fig. 5. At low tension, in the complete budding phase ($x = 1$), when increasing the tension, the radius decreases as

$$R = \frac{2\kappa_c R_c}{(\sigma - \mu_0)R_c + 2\kappa_c} \, , \tag{24}$$

which is derived from the condition, $\partial \mathcal{F}/\partial R(x = 1, R) = 0$. Once the boundary with the partial budding phase is crossed, increasing the tension has almost no effect on the radius R, while x decreases. As a conclusion, this model predicts that tension induces coat disassembling rather than flattening.

The elastic sheet model for the coat, Eq. (21), is certainly too simple to accurately describe important morphology change, which involves modifications of the internal molecular structure of the coat. Coat proteins can indeed adopt different arrangements to which correspond different radii [12, 23, 24, 40, 102, 123]. The polymerization energy $\mu(R)$ should thus have a discrete number of maximum, corresponding to allowed structures. Moreover, to go further on the study of the influence of the mechanical properties of the membrane on morphology selection, a kinetic description of coat growth is required [29]. The coat might be unable to reach the absolute free energy minimum, being kinetically trapped in some regions of the phase space. The membrane tension could not only affect the free energy of the different structures but also the height of the energy barriers separating them, allowing or not the coat to evolve toward a given structure.

4 Tubule Budding

Membrane tubules, with a radius of a few tens of nanometers and of several hundred nanometers long, are the second major type of transport carriers between the different cell compartments. Tubule budding is observed in the endoplasmic reticulum for transport toward the Golgi apparatus, in the Golgi for transport between the stacks of the Golgi and toward the endosomes or the plasma membrane, and in early and late endosomes for transport toward the plasma membrane or the Golgi, for a review see [75]. Three mechanisms can lead to tubule nucleation and growth from an initially flat membrane.

1. Application of a localized force normal to the membrane. This force can be generated by molecular motors bound to the membrane and walking along a microtubule, or by filaments pushing the membrane [21].
2. Polymerization on the membrane of proteins into a cylindrical rigid coat. Several proteins such as Dynamin, ESCRT III, Amphiphysin 1, and F-BAR domain have been found to form such cylindrical coats able to drive tubule formation [33,

41, 84, 98, 105]. The vesicle-generating coats COPI and COPII are also able to assemble into tubes [121, 123]. In vivo this mechanism could be involved for tubule formation in endosomes [16, 17] and for endoplasmic reticulum tubules stabilization [45].

3. High concentration of proteins inducing spontaneous curvature. Proteins that favor membrane bending, either by insertion of amphipathic helix [25, 57, 60], or by the binding of curved shape domains [11, 98], or by steric repulsion [99, 100], have all been observed to generate tubules.

In vivo several of the aforementioned basic mechanisms may come into play at the same time.

For the three mechanisms, the conditions required for the nucleation and growth of a single membrane tubule connected to a membrane of fixed tension are analyzed in the following. The shape of a tubule comprises a nearly cylindrical tube, the tip closing the tubule, and the neck connecting the tube to the rest of the membrane. The force acting at the tubule tip (defined positive when it opposes elongation) is,

$$f = \frac{\partial \mathcal{F}}{\partial L} \tag{25}$$

where L is the tubule length and $\mathcal{F}$ its free energy. A tubule elongates if $f \leq f_{\text{ext}}$, where f_{ext} is an externally applied force generated by molecular motors or active rigid filaments, for example, and shrinks and disappears in the opposite case. In the absence of external force, the stability of a tubule is determined by the sign of f. For long tubule, the free energy contributions from the tip and from the neck are independent of the tubule length, and hence do not contribute to the force f. Long tubule can hence be modeled in a first approximation as cylindrical membrane connected to a membrane reservoir. Note that in the following the effect of a pressure difference on each side of the membrane is neglected.

4.1 Tubule Pulled by an External Force

Pulling on a small area of a large membrane leads, at large displacement, to tubule formation [20, 42, 43, 76, 78]. The free energy of a tubule pulled from a membrane with no spontaneous curvature ($C_0 = 0$) and connected to a membrane reservoir of tension σ can be obtained from Eq. (1) by approximating the tubule shape as a cylinder of length L and radius R (the principal curvatures are thus $C_1 = 0$ and $C_2 = 1/R$),

$$\mathcal{F} = \left(\frac{\kappa}{2R^2} + \sigma \right) 2\pi R L \ . \tag{26}$$

The radius is not fixed a priori but minimizes $\mathcal{F}$,

$$R = \sqrt{\frac{\kappa}{2\sigma}} . \tag{27}$$

The force opposing tube elongation, defined by (25), is then,

$$f = 2\pi \sqrt{2\kappa\sigma} . \tag{28}$$

This is the force that has to be applied at the tip to stabilize the tubule. When the externally applied force is larger, $f_{ext} > 2\pi\sqrt{2\sigma\kappa}$, the tube elongates; for smaller force the tubule shrinks and collapses. The larger the tension, the thinner is the tubule and the larger is f. Taking $\kappa = 10^{-19}$ J and $10^{-6} < \sigma < 10^{-3}$ N/m, the radius and force are in the range $8 < R < 200$ nm and $5 < f < 100$ pN.

Under the cylindrical tube approximation and assuming a constant membrane tension independent of the tube length, the force f is independent of the length. This prediction is certainly valid at large L but should fail at early stage of tubule formation. To get more insight on the tubule shape and nucleation process, one has to solve Eqs. (2), (4) governing the shape of the membrane. The tubule shape computed numerically for different pulling forces f is shown in Fig. 6. In the neck region, far from the tube $r \gg R$, the rigidity has a negligible influence. The shape equation (4) reduces to $\sigma \sin \psi + f/2\pi r = 0$ and the shape is thus approximately a catenoid [76],

$$\psi = \arcsin\left(-\frac{f}{2\pi\sigma r}\right) \quad \text{for } r \gg R . \tag{29}$$
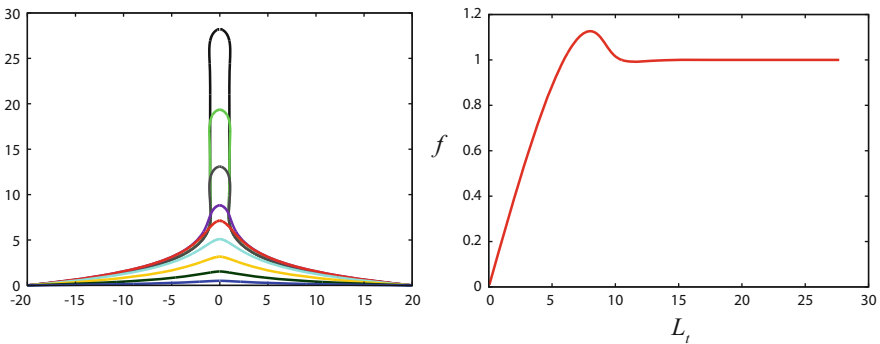

Fig. 6 Left: Tubules formed by applying punctual forces of different magnitudes at the center of a membrane disk connected to a reservoir, $f/2\pi\sqrt{2\kappa\sigma} = 0.1$ (blue), 0.3 (dark green), 0.6 (orange), 0.9 (sky blue), 1.1 (red), 1.1 (purple), 0.9965 (grey), 1 (green), 1 (black). The unit length is $\sqrt{\kappa/2\sigma}$. Right: force f (in $2\pi\sqrt{2\kappa\sigma}$ unit) at the tubule tip as a function of the total tubule length (from the disk edge to the tip)

(We remind that ψ and r characterizing the membrane shape are defined in Fig. 1.) When f is large enough, a tubular shape emerges. The tube is not perfectly cylindrical but shows small amplitude oscillations of the radius near the tip and neck. The force required to sustain the tubule as a function of the total tubule length, shown in Fig. 6, is non-monotonous. The force reaches a plateau $f = 2\pi\sqrt{2\kappa\sigma}$ at large length as predicted, but in order to nucleate the tube, a force larger by 13% has to be applied. See [20] for a more detailed analysis.

In vivo the force can be generated by molecular motors bound to the membrane and to microtubules or to actin filaments. Formation of tubules at the endoplasmic reticulum and the Golgi in particular requires molecular motors and microtubules [18, 26, 114, 117]. Membrane tubules can be produced in minimal artificial system with GUV containing motors in contact with a microtubule or actin network [53, 58, 83, 120].

Motors are able to pull-out membrane tubules only if the retracting force f due to tension and rigidity (28) is lower than the maximum force f_c that the motors can exert. The cooperation of several motors is necessary when f exceeds the stall force of an individual motor. In this case, f_c not only depends on the motor stall force, but also on the density of motors bound to the membrane and on kinetic parameters characterizing the motor [53, 58, 83, 92, 120]. For example, kinesin motors form a dynamical cluster at the tubule tip, pulling together the tubule by moving along microtubule [53, 58]. The form of f_c in this case is discussed in Appendix 2. In the case of myosin 1b, a non-processive motor that binds actin with catch-bond property (the unbinding rate increases with tension), the behavior is more complex [120]. At low density of motors, tubule formation is prevented at large f and, more surprisingly because of the catch-bond effect, also prevented at low f.

4.2 Tubule Formation Driven by Rigid Coat Polymerization

Tubule can be generated by the polymerization of proteins into a cylindrical rigid coat, which imposes its shape to the membrane. As for spherical coats discussed in Sect. 3, tubule formation results in this case from the competition between the polymerization energy driving tubule growth and, tension and rigidity opposing growth. The free energy of tubule formation reads in this case,

$$\mathcal{F} = \left(\frac{\kappa}{2R^2} + \sigma - \mu\right)2\pi RL + \mathcal{F}_0 , \tag{30}$$

The first term is the energy of the coated tube, which comprises the membrane deformation cost and the polymerization energy with μ the free energy gained (per unit area) by the polymerizing proteins. The second term, $\mathcal{F}_0$, accounts for various energy contributions independent of L due to the coat boundary and to the membrane deformation outside the coated tube. The radius R is imposed by the

coat. The force opposing tube elongation (25) reads,

$$f = -2\pi R \mu + 2\pi R \sigma + \frac{\pi \kappa}{R} \; ; \tag{31}$$

In the absence of an external force, the tubule elongates if f is negative, i.e., if,

$$\mu > \sigma + \frac{\kappa}{2R^2} \, , \tag{32}$$

and collapses in the opposite case. For a tubule of 20 nm radius, $\pi\kappa/R \simeq 10\,\mathrm{pN}$ and $2\pi\sigma R$ can vary in between 0.1 and 100 pN for plausible biological membrane tension. The polymerization energy depends on the coat protein interactions and on the concentration of proteins in the reservoir. For the protein dynamin, which assembles into tubes, the polymerization force has been measured in vitro, $2\pi R \mu \simeq 18\,\mathrm{pN}$ at a dynamin concentration of $12\,\mu\mathrm{M}$ [84]. Large tension can thus prevent dynamin tube growth. In vitro experiments with dynamin also confirmed the linear dependency of the tubule force f with the tension σ, and that at low dynamin concentration (i.e., low μ) the coat is not able to sustain the tubule.

In the presence of an external force, produced, for example, by motors, the growth condition is $f < f_{\mathrm{ext}}$. Even if the external force opposes growth ($f_{\mathrm{ext}} < 0$), a tubule can grow provided that the polymerization energy is large enough.

The constant energy term $\mathcal{F}_0$ in (30) generates a nucleation barrier: even if the condition (32) is fulfilled, the initial formation of a short tubule may be energetically unfavored ($\mathcal{F} > 0$). The nucleation of a coat with short length ℓ (of the order of the size of the assembling proteins) occurs only if the polymerization energy is large enough so that the energy $f\ell + \mathcal{F}_0$ is negative or not much larger than $k_{\mathrm{B}}T$. The free energy $\mathcal{F}_0$ includes different contributions,

$$\mathcal{F}_0 = \mathcal{F}_{\mathrm{b}} + \mathcal{F}_{\mathrm{tip}} + \mathcal{F}_{\mathrm{neck}} \, . \tag{33}$$

The first term is the loss of binding energy of the proteins at the coat boundaries. The second and third terms arise from the membrane deformation induced by the coat in the tip and neck region, respectively. In these regions, the membrane shape is obtained by solving Eqs. (2), (4), with the angle $\psi = \pi/2$ imposed by the coat at its border. For a tubule emerging from an initially flat membrane, $\mathcal{F}_{\mathrm{tip}}$ and $\mathcal{F}_{\mathrm{neck}}$ can be estimated, in the small and large tension limits, using the results of Sect. 3.1,

$$\mathcal{F}_{\mathrm{tip}} \simeq \begin{cases} 4\pi\kappa \\ 4\pi R\sqrt{2\kappa\sigma} \end{cases}, \mathcal{F}_{\mathrm{neck}} \simeq \begin{cases} \pi\sigma R^2 \left(-\gamma_e + \frac{1}{2} - \ln(4R\sqrt{\sigma/\kappa}) \right) & R^2\sigma/\kappa \ll 1 \\ 4\pi R\sqrt{2\kappa\sigma} & R^2\sigma/\kappa \gg 1 \end{cases} \tag{34}$$

For the neck, the shape and energy are the same as those reported in Sect. 3.1 and 3.2 in the case $x = 1/2$ or $\alpha = \pi/2$. For the tip, neglecting the tension, the equilibrium membrane shape is a hemisphere of radius R. Its bending energy is thus $4\pi\kappa$. At

large tension ($R^2\sigma/\kappa \gg 1$), the membrane is highly curved very near the coat edges and flat elsewhere. As discussed in Sect. 3.1.3, the deformation is almost unidimensional and the energy should be approximately same in the tip and in the neck.

The nucleation energy is much reduced if the coat nucleates in already deformed membrane with nearly tubular shape, in particular on the membrane neck connecting a budding vesicle to the rest of the membrane. If the neck radius matches the coat radius, $\mathcal{F}_{\text{neck}}$ and $\mathcal{F}_{\text{tip}}$ vanish. This could explain why, in cell, dynamin or ESCRT proteins assemble only at the neck of budding vesicles. In other membrane regions, the nucleation barrier might be too large to be counter-balanced by the polymerization energy. To support this hypothesis, it has been observed that at physiological concentration, dynamin tube does not nucleate on flat membrane but can nucleate on already existing tubular membrane with appropriate radius [84].

4.3 Influence of Curvature-Inducing Proteins on Tubule Formation

We discuss finally the emergence of tubules on a membrane containing proteins able to bend the membrane. In the simplest approach, the effect of the proteins is to give rise to a spontaneous curvature C_0 of the membrane. Campelo et al. [10, 54] have shown theoretically that the spontaneous curvature induced by amphipathic helix insertion is proportional to the surface fraction ϕ of proteins bearing such helix, $C_0 = c\phi$ with $c \simeq 1\,\text{nm}^{-1}$, in a wide range of density. At low density, proteins with curved domains adhering on the membrane have the same effect [63] with $c = 0.15\,\text{nm}^{-1}$ for N-BAR domain [4]. When the spontaneous curvature is induced by the lateral pressure arising from the steric repulsion between the membrane-bound proteins, a simple calculation [99] gives $C_0 = -ph/\kappa$ where p is the lateral pressure and h the membrane half-thickness.

4.3.1 Tubule Formation on a Membrane with Spontaneous Curvature

Let's consider first that the membrane is homogeneously covered with a fixed surface fraction of curvature-inducing proteins that provide a spontaneous curvature to the membrane. The free energy associated with the formation of cylindrical membrane tube with curvatures $C_1 = 0$ and $C_2 = 1/R$ and length L, budding on (and connected to) a flat membrane with tension σ, is obtained from (1) [21, 125],

$$\mathcal{F} = \left(\frac{\kappa}{2R^2} - \frac{\kappa C_0}{R} + \sigma \right) 2\pi R L \qquad (35)$$

The equilibrium radius and the retracting force (25) are then,

$$R = \sqrt{\frac{\kappa}{2\sigma}} , \quad f = 2\pi\kappa \left(\frac{1}{R} - C_0\right) . \tag{36}$$

Proteins inducing positive spontaneous curvature favor tubule budding. The larger the spontaneous curvature, the smaller the force f required to sustain the tube. The force vanishes when RC_0 approaches one.

Equation (36) suggests that a tube could spontaneously grow in the absence of external force if $1/R < C_0$, i.e., if $\sigma < \kappa C_0^2/2$. However, in this case a membrane tube is no longer stable (in the absence of pressure difference on each side of the membrane). The shape in this case should rather be a necklace of spheres [8, 21, 63, 89, 111, 112, 124] connected each other by a very thin neck. A cylindrical tube cannot spontaneously emerge in a membrane with (isotropic) spontaneous curvature without external force. Yet, the spontaneous curvature can strongly reduce the intensity of the required force.

4.3.2 Curvature–Concentration Coupling

In general, the density of proteins is not fixed and can be heterogeneous. Curvature-inducing proteins should concentrate in membrane regions with a curvature matching their preferential curvature, enhancing the local curvature.

The free energy functional of the local mean curvature $2H = C_1 + C_2$ and local surface concentration of proteins, ϕ, of a membrane piece of tension σ in contact with a reservoir of proteins is,

$$\mathcal{F}_{\mathrm{m}} = \int_A \left[\frac{\kappa(\phi)}{2}\big(2H - C_0(\phi)\big)^2 + g(\phi) + \sigma\right] dA , \tag{37}$$

where $g(\phi)$ is the free energy per unit area of the proteins on a flat membrane. Neglecting protein–protein interaction, this term reads,

$$g(\phi) = k_{\mathrm{B}}T\rho\big[\phi \ln \phi + (1 - \phi) \ln(1 - \phi)\big] - \mu_0\rho\phi , \tag{38}$$

where the first term is the mixing entropy with ρ, the inverse of the area of a molecule, and μ_0 is the difference between the chemical potential of the protein reservoir and the binding energy of a protein. At equilibrium, the local fraction of proteins minimizes the free energy, $\delta\mathcal{F}_{\mathrm{m}}/\delta\phi = 0$. The ϕ-dependence of C_0 and κ couples the equilibrium density to the equilibrium curvature. The density of proteins depends on the local curvature. In the case of a tubule connected to flat membrane reservoir, the density on the tube and on the flat membrane is different.

The free energy associated with the formation of a cylindrical membrane tube with surface fraction ϕ of proteins, radius R, and length L from a flat membrane

with surface fraction ϕ_0 of proteins is,

$$\mathcal{F} = \left(\frac{\kappa(\phi)}{2R^2} - \frac{\kappa(\phi)C_0(\phi)}{R} + \bar{g}(\phi) + \sigma \right) 2\pi R L , \qquad (39)$$

where $\bar{g}(\phi) = g(\phi) - g(\phi_0) + \kappa(\phi)C_0(\phi)^2/2 - \kappa(\phi_0)C_0(\phi_0)^2/2$. The surface fraction in the flat membrane reservoir satisfies $\bar{g}'(\phi_0) = 0$, where the prime denotes the derivative respect to ϕ.

If the case of a weak density-curvature coupling, the free energy density in (37) can be expanded at the quadratic order in H and ϕ by assuming,

$$\kappa(\phi) = \kappa , \quad \bar{g}(\phi) = \frac{\chi}{2}(\phi - \phi_0)^2 , \quad C_0(\phi) = C_0(\phi_0) + c(\phi - \phi_0) , \qquad (40)$$

where according to (38), $\chi = \frac{k_B T \rho}{\phi_0(1-\phi_0)} + \kappa c^2$. One then recovers Leibler's model [61, 62], which yields, using $\delta \mathcal{F}_m / \delta \phi = 0$, a linear relation between the deviation of the protein surface fraction and the curvature,

$$\phi - \phi_0 = \frac{2\kappa c}{\chi} H . \qquad (41)$$

Inserting (40) and (41) with $2H = 1/R$ in (39), the free energy of tube formation is the same as (35) replacing C_0 by $C_0(\phi_0)$ and κ by an effective rigidity $\tilde{\kappa} = \kappa \left(1 - \kappa c^2/\chi \right)$. Doing the same replacements in (36), one obtains the equilibrium radius R and force f. The radius scales as $\sim \sigma^{-1/2}$ as in the absence of proteins. The force is an affine function of $\sqrt{\sigma}$ vanishing at a finite tension. All these features have been observed experimentally in vitro on membrane tubules pulled from GUV and covered by amphiphysin proteins [98]. The authors obtained $1/c$ of the order of 1–5 nm.

Figure 7 shows the tubule shape computed numerically, in the weak coupling approximation (40) for two different values of $RC_0(\phi_0)$. When $RC_0(\phi_0)$ approaches 1 (right panels), the tube resembles a sphere necklace at small length. At larger L, the tube is nearly cylindrical at the center but keeps an undulating shape at the extremities. The force f needed to pull the tube drops when $RC_0(\phi_0) \to 1$, as predicted. As already discussed, for $RC_0(\phi_0) < 1$ a tube is no longer stable. Figure 7 shows also the protein density along the tube: $\phi = \phi_0$ at the basis and $\phi \simeq \phi_0 + \kappa c / \chi R$ in the tube.

4.3.3 Anisotropic Spontaneous Curvature

Proteins with crescent shape, such as those with a BAR domain, induce anisotropic deformation of the membrane in their vicinity and their orientation is coupled to the local curvature of the membrane. For strong coupling, an orientational order should appear favoring anisotropic bending of the membrane [31, 56]. Simulations of membrane containing anisotropic curvature-inducing proteins [4, 73, 77] show
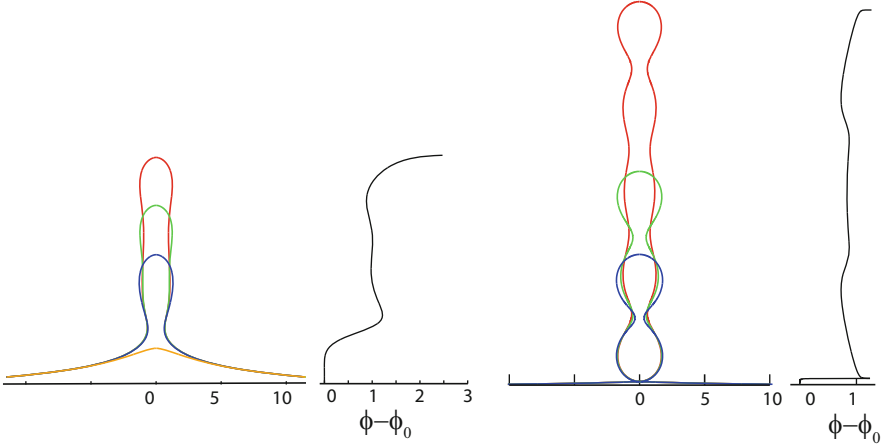
Fig. 7 The color curves show the contour of a tubule at different elongations L obtained by applying a normal punctual force f to a flat membrane containing curvature-inducing proteins. The black curves show $\phi - \phi_0$ function of z. Two sets of parameters have been used. Left: $(\kappa/\tilde{\kappa})RC_0(\phi_0) = 0.5$ and $f/2\pi\sqrt{\sigma\tilde{\kappa}} = 0.5$. Right: $(\kappa/\tilde{\kappa})RC_0(\phi_0) = 0.95$ and $f/2\pi\sqrt{\sigma\tilde{\kappa}} = 0.05$. The unit of length is R given by (36) and the unit of ϕ is $\kappa c/\chi R$

that the proteins aggregate because of curvature-mediated interactions, forming dense nematic phase domains. In these domains, the membrane is strongly curved and often adopts a tubular shape. Thus, unlike proteins inducing isotropic curvature, proteins inducing anisotropic curvature are able to drive stable tubule formation in the absence of external force.

In a nematic ordered phase the elastic free energy of the membrane with the proteins comprises additional terms, as compared with (1), favoring anisotropic bending [31, 56]. Different equivalent formulations can be found in the literature [32, 77, 115]. Using the expression of [77] it reads,

$$\mathcal{F}_{\mathrm{m}} = \int_A \left[\frac{\kappa}{2}(2H)^2 + \frac{\kappa_\parallel}{2}(C_\parallel - C_{0\parallel})^2 + \frac{\kappa_\perp}{2}(C_\perp - C_{0\perp})^2 + \sigma \right] dA + \mathcal{F}_{\mathrm{nematic}}, \quad (42)$$

where $2H = C_1 + C_2$, $C_\parallel$ and $C_{0\parallel}$ are the curvature and spontaneous curvature in the direction of the nematic director $\mathbf{n}$, $C_\perp$ and $C_{0\perp}$ are the curvature and spontaneous curvature in the direction normal to $\mathbf{n}$, and $\kappa_\parallel$ and $\kappa_\perp$ are bending moduli. The last term $\mathcal{F}_{\mathrm{nematic}}$ accounts for the heterogeneity of the nematic orientation.

The free energy of a cylindrical membrane tube with homogeneous nematic director orientation characterized by the angle θ with the orthoradial direction budding from a flat membrane with nematic order is,

$$\mathcal{F} = \left[\frac{\kappa}{2R^2} + \frac{\kappa_\parallel \cos^4\theta}{2R^2} - \frac{\kappa_\parallel C_{0\parallel}\cos^2\theta}{R} + \frac{\kappa_\perp \sin^4\theta}{2R^2} - \frac{\kappa_\perp C_{0\perp}\sin^2\theta}{R} + \sigma \right] 2\pi RL. \quad (43)$$

The analysis of the tube properties can be found in [77]. Here for simplicity, only the simple case with $\kappa_\perp = 0$ is analyzed. Minimizing the energy (43) with respect to θ and R, and computing the force (25), one obtains,

$$\cos^2 \theta = C_{0\parallel} R \,, \quad R = \sqrt{\frac{\kappa}{2\sigma - \kappa_\parallel C_{0\parallel}^2}}, \quad f = \frac{2\pi\kappa}{R} \,, \quad \text{for } RC_{0\parallel} \leq 1 \,,$$

$$\cos^2 \theta = 1 \,, \quad R = \sqrt{\frac{\kappa + \kappa_\parallel}{2\sigma}}, \quad f = 2\pi(\kappa + \kappa_\parallel)\left(\frac{1}{R} - \frac{\kappa_\parallel}{\kappa + \kappa_\parallel}C_{0\parallel}\right),$$

$$\text{for } RC_{0\parallel} \geq 1 \,, \qquad (44)$$

At large tension (first line), the tube principal curvature is larger than the spontaneous curvature, the proteins can orientate so that the curvature along their direction matches the spontaneous curvature. Thus interestingly, the orientation depends on the tension at large tension. When $R = 1/C_{0\parallel}$, the proteins orientate perpendicular to the tube direction. The proteins keep this orientation at lower tension (second line), when the radius is too large for $C_\parallel$ to match $C_{0\parallel}$. The force vanishes at finite tension $2\sigma = \kappa_\parallel^2 C_{0\parallel}^2/(\kappa_\parallel + \kappa)$, implying the spontaneous growth of tubule at lower tension. To go further in the study of the shape and stability of tubes formed in membrane with anisotropic spontaneous curvature requires the analysis of the shape equations, which have been derived in [115].

5 Membrane Fusion in Intracellular Trafficking

After budding from a donor compartment, transport vesicles and tubules travel in the cell and eventually fuse with the membrane of the target compartment. The fusion process is discussed in more detail in chapter "Common Energetic and Mechanical Features of Membrane Fusion and Fission Machineries." In this section, we focus on the influence of the membrane tension in the fusion of intracellular vesicles.

Lipid bilayers are very stable objects that do not fuse spontaneously in general. Unlike the budding process described before, the fusion of two membranes requires major rearrangements of the molecules with the formation of several intermediate structures during the fusion process. These metastable structures are separated by energetic barriers that have to be overcome for fusion to succeed (a schematic view of the different barriers deduced from molecular simulations works is proposed in [65]). In vivo the fusion of intracellular vesicles is ensured by an energy consuming protein machinery, the SNARE complex, which can alone trigger fusion [118], possibly assisted by other proteins [13, 71]. Though the exact way by which SNAREs mediate fusion is still under debate, it is believed that the main role of the SNARE complex is to act as a pin that pulls on the two membranes to put them in very close proximity.

Because fusion involves processes taking place at the molecular level, its study is rather challenging both theoretically and experimentally. On the theoretical side, continuum media approaches such as those used in Sects. 3 and 4 to study budding are of more limited predictive power [55]. Much insights have been gained this last decade by the use of molecular simulations, see [65] for a review, and see [81, 82] for discussions, based on simulation results, on the role of SNARE. The current understanding of the fusion pathways that emerges from simulation studies is summarized in [87].

5.1 Influence of Membrane Tension on Fusion Barriers

Experimental and numerical studies show that membrane tension facilitates membrane fusion. This was first observed in experiments in which the fusion of protein-free membranes was induced by rising the membrane tension by the osmotic swelling of the fusing vesicles [15, 27]. More recently, it has been shown that vesicles stably adhering on a flat lipid bilayer fuse with the bilayer when an extensile strain is applied to the bilayer [103]. The spontaneous fusion of lipid bilayers triggered by high tension has been reproduced in molecular simulations [94]. Simulations, using dissipative particles dynamics, also showed that the average duration of the fusion process decreases exponentially with the tension [38, 39]. Some energy barriers encountered in the fusion process are thus lowered when tension increases.

Tension most probably facilitates the early stage of fusion, from the unfused membranes to the formation of the metastable intermediate structure named "the stalk" [39, 81]. In the first step of fusion, the two membranes have to come in close proximity (a few nm), which is prevented by entropic and hydration repulsion. According to [59], the energy cost of stalk formation rapidly increases when the distance between the membrane increases. Increasing the tension by stretching the membrane and lowering the lipid density should increase the hydrophobicity of the membranes and then decrease the repulsion between the two membranes, thereby helping to cross the first barrier. In the next step identified in simulations prior to stalk formation, few lipids establish bridges between the two facing monolayers by adopting a splayed conformation with each of their tail inserted in a different leaflet, [82, 96, 104]. This prestalk configuration involves the transient exposure of lipid tails to the aqueous solvent and thus the crossing of an energetic barrier. This barrier should also be lower for membrane with higher tension where the area per lipid is larger. Dissipative particle simulations confirm this statement and show that the energy barrier for prestalk formation decreases linearly with tension [38, 39].

Though high tension reduces the height of the fusion barrier, it is still not known whether tension significantly affects the fusion kinetic in the presence of the SNARE machinery. Experimental studies in this direction using simple biomimetic systems would be interesting. In living cells different studies showed that exocytosis (the fusion of intracellular vesicles with the plasma membrane) is stimulated by high

tension [35, 72]. For example, during the growth of plant cells the increase of tension due to cell expansion is believed to trigger the fusion of vesicles in order to incorporate membrane material [72]. The increase of exocytosis activity may be linked to the fact that tension facilitates membrane fusion.

5.2 Transport Driven by Tension Gradient

In analogy with fluid flowing from high pressure to low pressure regions, tension gradients can induce flow inside fluid membranes from low tension toward high tension regions. Such gradients can appear after the fusion of two membranes with different tensions, leading to a flow of membrane molecules in the fusion pore region. The area flux is obtained from the balance of the work produced by the tension difference $\Delta\sigma$ per time unit and the dissipated energy. It has been calculated in [14] for a toroidal pore and in [22] for a long tubular pore,

$$ J = \frac{2\pi R^2 \Delta\sigma}{\tilde{\eta}} \tag{45} $$

where R is the pore radius and $\tilde{\eta}$ a 2D viscosity which comprises the different sources of dissipation. For the toroidal pore the dissipation is dominated by the membrane intrinsic viscosity η_s and the friction between the two monolayers μ,

$$ \tilde{\eta} = \eta_s a + \eta_r b , \tag{46} $$

where a and b are dimensionless geometrical factors, and $\eta_r = \mu h^2$ with h the membrane thickness. The typical values of biological membrane viscosity are in the range $\eta_s \sim 10^{-8}-10^{-9}$ kg/s. The viscosity due to inter-layer friction η_r is less well characterized and usually smaller than η_s. For $R = 10$ nm and a realistic tension difference $\Delta\sigma \sim 10^{-5}$ N/m [113], one obtains a flux of the order $J \sim 0.1-1\,\mu m^2$/s, i.e., a velocity in the pore $v \sim 10\,\mu m^2$/s. For a long cylindrical tubule with length L, the dissipation is mainly due to the viscosity of the surrounding fluid η, and thus,

$$ \tilde{\eta} = \frac{4\eta L}{\ln(L/R) - 1/2} . \tag{47} $$

The flow of membrane drags the fluid in the membrane vicinity leading to a flow of fluid through the pore. Note that the tension gradient also generates a pressure gradient because of the Laplace law, leading to a (smaller) counter-flow. The detailed calculation for a long tubule has been done in [22]. It shows that the net flux of fluid in the tubule is oriented in the same direction as the membrane flux: toward the high tension region. This mechanism allows membrane molecules of the lumen to be pumped from one organelle at low tension toward another at higher tension.

Tension-induced flow might be a powerful way to transport material between two organelles, for instance, through tubules bridging the two membranes. It is faster than diffusion and provides a directionality, crucial in intracellular trafficking. This phenomenon has first been invoked in living cell to explain the absorption of the Golgi apparatus by the ER in cells treated with Brefeldin A [88]. The measure of the difference of the membrane tension between the Golgi and the ER strengthens this hypothesis and more generally the relevance of the mechanism in intracellular trafficking [113]. It might be at work in particular for the transport inside the Golgi [37], where tubular connections between *cisterna* have been observed [66, 110].

6 Intracellular Traffic Regulation by Tension

The mechanical properties of the membrane and in particular the tension affect the elementary processes of intracellular trafficking. Vesicle and tubule budding is prevented at high tension and high tension favors membrane fusion. On the other hand, tension is directly related to membrane area change. Fusion of vesicles brings area to the membrane of the receptor compartment, which should lead to the decrease of its tension. Reversely, vesicle budding and fission by removing area from the donor compartment should increase its tension. The influence of fusion and budding on membrane tension has been observed in in vitro experiments. The tension of GUV fusing with small vesicles drops eventually leading to the membrane destabilization [97]. In lipid droplets the secretion of small vesicles (produced by COPI coat) increases the tension of the droplet until vesicle budding is no longer possible [108]. In the same manner, the unexpected relationship observed in [99] between the length and radius of tubules budding on GUV and the initial volume of GUV revealed that GUV tension increases during tubule growth until the threshold tension of tubule growth is reached.

The mutual influence between the fusion and production of transport vesicles and tubules, and the value of the tension of the donor/target compartment suggests that tension could be a major regulator of intracellular trafficking. It could coordinate the release and entry of transport vesicles and tubules in a compartment. Successive fusions by lowering the tension could trigger tubules or vesicle production [97]. At the opposite, successive vesicle or tubule budding could increase the tension enough to stop further secretion and favor fusion. Such feedback would ensure the compartment stability.

The coordination of material absorption and release is crucial for the intracellular compartments named endosomes. They are sorting platforms that collect, sort, and then send to the proper location of the endocytosed material. For this purpose, they fuse with small vesicles internalized by the cell and release the sorted molecules in different tubules and vesicles. Endosomes work in a collective manner frequently fusing each other [30, 80]. Tension could partly coordinate their activity, allowing vesicle and tubule release only when enough fusion processes have taken place (lowering the tension below the budding threshold) and brought material to be sorted

and released. In order to meet and fuse, endosomes move inside the cell, pulled by molecular motors along cell filaments. Depending on the endosome membrane tension, motor pulling on membrane could either induce tubule budding at low tension, or induce motion when the membrane is stiffer at high tension. It is thus possible that the succession of motion–fusion–tubule release–motion realized by endosomes is regulated to some extent by the endosome tension. High tension would lead to endosome motion until its fusion with another endosome. The resulting drop of the tension would then favor tubule release until the tension has increased again.

Lipid droplets provide another example of cell compartment where tension may have a regulatory role. Lipid droplets are in charge of the storage and on-demand delivery of neutral lipids [67, 109]. COPI coats assemble on their membrane (a monolayer in this case) leading to vesicle release. It has been proposed that the goal of this vesicle secretion is to increase the droplet tension in order to put the droplet in a highly fusogenic state [108, 119]. The membrane of the droplet would then be able to spontaneously fuse with that of the endoplasmic reticulum and create the observed bridges between the two organelles. Such bridge could permit the transfer of enzymes from the endoplasmic reticulum to the lipid droplets, possibly assisted by the tension gradient.

Tension may also be an important physical regulator of the plasma membrane dynamics [36]. Exocytosis (fusion of the plasma membrane with intracellular vesicles) and endocytosis (production of intracellular vesicles by the plasma membrane) are known to be influenced by the membrane tension [35, 72, 79]. They also participate to membrane area regulation, and thus tension regulation, even if in the case of the plasma membrane, tension is also controlled to a large extent by the cytoskeleton and area reservoirs such as caveolae [95]. Tension may also correlate trafficking to other mechanosensitive processes such as cell adhesion and motility [36].

Appendix 1: Shape Equations for Axisymmetric Membrane

The shape of a membrane with cylindrical symmetry can be characterized by the functions $r(s)$, $z(s)$, and $\psi(s)$, where s is the arc length along the shape contour in a plane at a fixed azimuthal angle. r and z are the usual cylindrical coordinates and ψ is the angle between the radial and the tangent vectors, see Fig. 2.

In the most general case in which the membrane undergoes a pressure difference between each side and a force pulling along the z-axis at the contour boundaries, the shape of the membrane minimizes the free energy,

$$\mathcal{G} = \mathcal{F}_\mathrm{m} - pV - fL \,, \tag{48}$$

The second term is the energy cost associated with the volume change with $V = \pi \int_0^{s_1} r^2 \sin\psi \, ds$ the volume enclosed by the membrane and p the pressure difference across the membrane. The last term is included when $L = z(0) - z(s_1) =$

$\int_0^{s_1} \sin \psi \, ds$ is fixed; f is then the force exerted by the membrane at $s = 0$ and $s = s_1$ in the z direction.

In order to minimize $\mathcal{G}$ with respect to $r(s)$ and $\psi(s)$ accounting for the constrain (2), one has to introduce a Lagrange multiplier $\gamma(s)$ and minimize the functional,

$$S[r(s), \psi(s)] = \frac{\mathcal{G}}{2\pi\kappa} + \int_0^{s_1} \gamma(s)(\dot{r} - \cos\psi)ds = \int_0^{s_1} \mathcal{L}(\psi, \dot{\psi}, r, \dot{r})ds \quad (49)$$

with,

$$\mathcal{L} = \frac{1}{2}\left(\dot{\psi} + \frac{\sin\psi}{r} - C_0\right)^2 r + \frac{\sigma}{\kappa}r - \frac{p}{2\kappa}r^2 \sin\psi - \frac{f}{2\pi\kappa}\sin\psi + \gamma(\dot{r} - \cos\psi) \quad (50)$$

The condition $\delta S = 0$ leads to the Euler–Lagrange equations $\frac{\partial \mathcal{L}}{\partial r} - \frac{d}{ds}\frac{\partial \mathcal{L}}{\partial \dot{r}} = 0$ and $\frac{\partial \mathcal{L}}{\partial \psi} - \frac{d}{ds}\frac{\partial \mathcal{L}}{\partial \dot{\psi}} = 0$,

$$\ddot{\psi} = -\frac{\dot{\psi}\cos\psi}{r} + \frac{\cos\psi\sin\psi}{r^2} - \frac{p}{2\kappa}r\cos\psi + \frac{\gamma\sin\psi}{r} - \frac{f}{2\pi\kappa}\frac{\cos\psi}{r},$$

$$\dot{\gamma} = \frac{1}{2}\left(\dot{\psi} - C_0\right)^2 - \frac{1}{2}\frac{\sin^2\psi}{r^2} + \frac{\sigma}{\kappa} - \frac{p}{\kappa}r\sin\psi, \quad (51)$$

and to the boundary conditions at $s = 0$ and $s = s_1$,

$$\psi \text{ fixed or } \frac{\partial \mathcal{L}}{\partial \dot{\psi}} = \dot{\psi} + \frac{\sin\psi}{r} - C_0 = 0,$$

$$r \text{ fixed or } \frac{\partial \mathcal{L}}{\partial \dot{r}} = \gamma = 0. \quad (52)$$

Equation (51) together with Eq. (2) forms a close set of differential equations of 4th order complemented by four boundary conditions (52).

In the usual case where the contour length s_1 is not fixed, then $H = \dot{r}\partial_{\dot{r}}\mathcal{L} + \dot{\psi}\partial_{\dot{\psi}}\mathcal{L} - \mathcal{L} = 0$, which gives,

$$\frac{r\dot{\psi}^2}{2} - \frac{r}{2}\left(\frac{\sin\psi}{r} - C_0\right)^2 - \frac{\sigma}{\kappa}r + \frac{p}{2\kappa}r^2\sin\psi + \gamma\cos\psi + \frac{f}{2\pi\kappa}\sin\psi = 0. \quad (53)$$

This equation can be combined with (51) to eliminate γ and obtain a lowest order equation in ψ and r, Eq. (4).

Appendix 2: Model for Dynamical Cluster of Kinesin at Tubule Tip

The force f required to pull a tubule is usually larger than the stall force $f_s \sim 10\,\text{pN}$ of a single motor. Several motors, localized at the tip of the tubule, then work cooperatively to extract a tube [53, 58]. Tubule formation then relies on two conditions: (1) the formation of a stable cluster of N motors at the tip, and (2) the load on each motor (f/N assuming that the force created by the membrane is equally distributed among the motors) should be smaller than the stall force. Let's consider the first condition. A cluster of motors at the tubule tip is sustained by an influx J_b of motors moving along the tube, and looses motors that unbind the microtubule at a rate dependent of their load, $k_u \exp\left(\frac{fa}{Nk_BT}\right)$, where k_u is the unbinding rate at zero load and a is the typical distance of the motor–microtubule interaction. The influx J_b depends on the density of motors on the membrane, and kinetic parameters such as the motor velocity, the binding and unbinding rates [53, 58]. The flux balance,

$$k_u N \exp\left(\frac{fa}{Nk_BT}\right) = J_b \,, \tag{54}$$

determines N, the number of motors in the cluster. A stable cluster can exist only if $\frac{J_b k_B T}{k_u} fa > e$ where $e \simeq 2.71$ is the base of natural logarithm. In this case, N is in the range $\frac{J_b}{k_u} < N < \frac{J_b}{k_u}e$. Then accounting for the second condition, $f/N < f_s$, tubule extraction by the collective action of molecular motors is possible if the force f (28) exerted by the membrane is lower than a critical value,

$$f < f_c \quad \text{with}\,, \quad f_c = \begin{cases} \frac{k_B T}{a}\frac{J_b}{k_u}\frac{1}{e} & \text{if } f_s a > k_B T \\ f_s \frac{J_b}{k_u} \exp\left(-\frac{f_s a}{k_B T}\right) & \text{if } f_s a < k_B T \end{cases} \tag{55}$$

References

1. Agrawal NJ, Nukpezah J, Radhakrishnan R (2010) Minimal mesoscale model for protein-mediated vesiculation in clathrin-dependent endocytosis. PLoS Comput Biol 6(9):e1000926
2. Alberts B, Johnson A, Lewis J, Morgan D, Raff M, Roberts K, Walter P (2014) Molecular biology of the cell, 6th edn. Garland, New York
3. Antonny B (2006) Membrane deformation by protein coats. Curr Opin Cell Biol 18(4):386–394
4. Ayton GS, Blood PD, Voth GA (2007) Membrane remodeling from n-bar domain interactions: insights from multi-scale simulation. Biophys J 92(10):3595–3602
5. Beck R, Ravet M, Wieland FT, Cassel D (2009) The COPI system: molecular mechanisms and function. FEBS Lett 583(17):2701–2709
6. Bonifacino JS, Glick BS (2004) The mechanisms of vesicle budding and fusion. Cell 116(2):153–166

7. Boulant S, Kural C, Zeeh J-C, Ubelmann F, Kirchhausen T (2011) Actin dynamics counteract membrane tension during clathrin-mediated endocytosis. Nat Cell Biol 13(9):1124–1131

8. Bukman DJ, Yao JH, Wortis M (1996) Stability of cylindrical vesicles under axial tension. Phys Rev E 54(5):5463

9. Cai H, Reinisch K, Ferro-Novick S (2007) Coats, tethers, Rabs, and SNAREs work together to mediate the intracellular destination of a transport vesicle. Dev Cell 12(5):671–682

10. Campelo F, McMahon HT, Kozlov MM (2008) The hydrophobic insertion mechanism of membrane curvature generation by proteins. Biophys J 95(5):2325–2339

11. Carlton J, Bujny M, Peter BJ, Oorschot VMJ, Rutherford A, Mellor H, Klumperman J, McMahon HT, Cullen PJ (2004) Sorting nexin-1 mediates tubular endosome-to-TGN transport through coincidence sensing of high-curvature membranes and 3-phosphoinositides. Curr Biol 14(20):1791–1800

12. Cheng Y, Boll W, Kirchhausen T, Harrison SC, Walz T (2007) Cryo-electron tomography of clathrin-coated vesicles: structural implications for coat assembly. J Mol Biol 365(3):892–899

13. Chernomordik LV, Kozlov MM Mechanics of membrane fusion. Nat Struct Mol Biol 15(7):675–683 (2008)

14. Chizmadzhev YA, Kumenko DA, Kuzmin PI, Chernomordik LV, Zimmerberg J, Cohen FS (1999) Lipid flow through fusion pores connecting membranes of different tensions. Biophys J 76(6):2951–2965

15. Cohen FS, Akabas MH, Finkelstein A (1982) Osmotic swelling of phospholipid vesicles causes them to fuse with a planar phospholipid bilayer membrane. Science 217(4558):458–460

16. Cullen PJ (2008) Endosomal sorting and signalling: an emerging role for sorting nexins. Nat Rev Mol Cell Biol 9(7):574–582

17. Cullen PJ, Korswagen HC (2012) Sorting nexins provide diversity for retromer-dependent trafficking events. Nat Cell Biol 14(1):29–37

18. Dabora SL, Sheetz MF (1988) The microtubule-dependent formation of a tubulovesicular network with characteristics of the ER from cultured cell extracts. Cell 54(1):27–35

19. den Otter WK, Briels WJ (2011) The generation of curved clathrin coats from flat plaques. Traffic 12(10):1407–1416

20. Derényi I, Jülicher F, Prost J (2002) Formation and interaction of membrane tubes. Phys Rev Lett 88(23):238101

21. Derényi I, Koster G, Van Duijn MM, Czövek A, Dogterom M, Prost J (2007) Membrane nanotubes. In: Controlled nanoscale motion. Springer, Berlin, pp 141–159

22. Dommersnes PG, Orwar O, Brochard-Wyart F, Joanny JF (2005) Marangoni transport in lipid nanotubes. Europhys Lett 70(2):271

23. Faini M, Prinz S, Beck R, Schorb M, Riches JD, Bacia K, Brügger B, Wieland FT, Briggs JAG (2012) The structures of COPI-coated vesicles reveal alternate coatomer conformations and interactions. Science 336(6087):1451–1454

24. Faini M, Beck R, Wieland FT, Briggs JAG (2013) Vesicle coats: structure, function, and general principles of assembly. Trends Cell Biol 23(6):279–288

25. Farsad K, Ringstad N, Takei K, Floyd SR, Rose K, De Camilli P (2001) Generation of high curvature membranes mediated by direct endophilin bilayer interactions. J Cell Biol 155(2):193–200

26. Feiguin F, Ferreira A, Kosik KS, Caceres A (1994) Kinesin-mediated organelle translocation revealed by specific cellular manipulations. J Cell Biol 127(4):1021–1039

27. Finkelstein A, Zimmerberg J, Cohen FS (1986) Osmotic swelling of vesicles: its role in the fusion of vesicles with planar phospholipid bilayer membranes and its possible role in exocytosis. Annu Rev Physiol 48(1):163–174

28. Foret L (2014) Shape and energy of a membrane bud induced by protein coats or viral protein assembly. Eur Phys J E 37(5):1–13

29. Foret L, Sens P (2008) Kinetic regulation of coated vesicle secretion. Proc Natl Acad Sci 105(39):14763–14768

30. Foret L, Dawson JE, Villaseñor R, Collinet C, Deutsch A, Brusch L, Zerial M, Kalaidzidis Y, Jülicher F (2012) A general theoretical framework to infer endosomal network dynamics from quantitative image analysis. Curr Biol 22(15):1381–1390

31. Fournier JB (1996) Nontopological saddle-splay curvature instabilities from anisotropic membrane inclusions. Phys Rev Lett 76(23):4436

32. Frank JR, Kardar M (2008) Defects in nematic membranes can buckle into pseudospheres. Phys Rev E 77(4):041705

33. Frost A, Perera R, Roux A, Spasov K, Destaing O, Egelman EH, De Camilli P, Unger VM (2008) Structural basis of membrane invagination by f-bar domains. Cell 132(5):807–817

34. Frost A, Unger VM, De Camilli P (2009) The bar domain superfamily: membrane-molding macromolecules. Cell 137(2):191–196

35. Gauthier NC, Fardin MA, Roca-Cusachs P, Sheetz MP (2011) Temporary increase in plasma membrane tension coordinates the activation of exocytosis and contraction during cell spreading. Proc Natl Acad Sci 108(35):14467–14472

36. Gauthier NC, Masters TA, Sheetz MP (2012) Mechanical feedback between membrane tension and dynamics. Trends Cell Biol 22(10):527–535

37. Glick BS, Nakano A (2009) Membrane traffic within the Golgi apparatus. Annu Rev Cell Dev Biol 25:113

38. Grafmüller A, Shillcock J, Lipowsky R (2007) Pathway of membrane fusion with two tension-dependent energy barriers. Phys Rev Lett 98(21):218101

39. Grafmüller A, Shillcock J, Lipowsky R (2009) The fusion of membranes and vesicles: pathway and energy barriers from dissipative particle dynamics. Biophys J 96(7):2658–2675

40. Gürkan C, Stagg SM, LaPointe P, Balch WE (2006) The COPII cage: unifying principles of vesicle coat assembly. Nat Rev Mol Cell Biol 7(10):727–738

41. Hanson PI, Roth R, Lin Y, Heuser JE (2008) Plasma membrane deformation by circular arrays of ESCRT-iii protein filaments. J Cell Biol 180(2):389–402

42. Heinrich V, Božič B, Svetina S, Žekš B (1999) Vesicle deformation by an axial load: from elongated shapes to tethered vesicles. Biophys J 76(4):2056–2071

43. Hochmuth RM, Wiles HC, Evans EA, McCown JT (1982) Extensional flow of erythrocyte membrane from cell body to elastic tether. II. experiment. Biophys J 39(1):83

44. Hsu VW, Lee SY, Yang J-S (2009) The evolving understanding of COPI vesicle formation. Nat Rev Mol Cell Biol 10(5):360–364

45. Hu J, Shibata Y, Voss C, Shemesh T, Li Z, Coughlin M, Kozlov MM, Rapoport TA, Prinz WA (2008) Membrane proteins of the endoplasmic reticulum induce high-curvature tubules. Science 319(5867):1247–1250

46. Hurley JH, Boura E, Carlson L-A, Różycki B (2010) Membrane budding. Cell 143(6):875–887

47. Jackson LP (2014) Structure and mechanism of COPI vesicle biogenesis. Curr Opin Cell Biol 29:67–73

48. Jin AJ, Prasad K, Smith PD, Lafer EM, Nossal R (2006) Measuring the elasticity of clathrin-coated vesicles via atomic force microscopy. Biophys J 90(9):3333–3344

49. Jülicher F, Seifert U (1994) Shape equations for axisymmetric vesicles: a clarification. Phys Rev E 49(5):4728

50. Kirchhausen T (2009) Imaging endocytic clathrin structures in living cells. Trends Cell Biol 19(11):596–605

51. Kirchhausen T (2000) Three ways to make a vesicle. Nat Rev Mol Cell Biol 1(3):187–198

52. Kirchhausen T (2012) Bending membranes. Nat Cell Biol 14(9):906–908

53. Koster G, VanDuijn M, Hofs B, Dogterom M (2003) Membrane tube formation from giant vesicles by dynamic association of motor proteins. Proc Natl Acad Sci 100(26):15583–15588

54. Kozlov MM, Campelo F, Liska N, Chernomordik LV, Marrink SJ, McMahon HT (2014) Mechanisms shaping cell membranes. Curr Opin Cell Biol 29:53–60

55. Kozlovsky Y, Kozlov MM (2002) Stalk model of membrane fusion: solution of energy crisis. Biophys J 82(2):882–895

56. Kralj-Iglič V, Heinrich V, Svetina S, Žekš B (1999) Free energy of closed membrane with anisotropic inclusions. Eur Phys J B 10(1):5–8
57. Krauss M, Jia J-Y, Roux A, Beck R, Wieland FT, De Camilli P, Haucke P (2008) Arf1-GTP-induced tubule formation suggests a function of Arf family proteins in curvature acquisition at sites of vesicle budding. J Biol Chem 283(41):27717–27723
58. Leduc C, Campàs O, Zeldovich KB, Roux A, Jolimaitre P, Bourel-Bonnet L, Goud B, Joanny J-F, Bassereau P, Prost J (2004) Cooperative extraction of membrane nanotubes by molecular motors. Proc Natl Acad Sci USA 101(49):17096–17101
59. Lee JY, Schick M (2007) Dependence of the energies of fusion on the intermembrane separation: optimal and constrained. J Chem Phys 127(7):075102
60. Lee MCS, Orci L, Hamamoto S, Futai E, Ravazzola M, Schekman R (2005) Sar1p N-terminal helix initiates membrane curvature and completes the fission of a COPII vesicle. Cell 122(4):605–617
61. Leibler S (1986) Curvature instability in membranes. J Phys 47(3):507–516
62. Leibler S, Andelman D (1987) Ordered and curved meso-structures in membranes and amphiphilic films. J Phys 48(11):2013–2018
63. Lipowsky R (2013) Spontaneous tubulation of membranes and vesicles reveals membrane tension generated by spontaneous curvature. Faraday Discuss 161:305–331
64. Manneville J-B, Casella J-F, Ambroggio E, Gounon P, Bertherat J, Bassereau P, Cartaud J, Antonny B, Goud B (2008) COPI coat assembly occurs on liquid-disordered domains and the associated membrane deformations are limited by membrane tension. Proc Natl Acad Sci 105(44):16946–16951
65. Markvoort AJ, Marrink SJ (2011) Lipid acrobatics in the membrane fusion arena. Curr Top Membr 68:259–294
66. Marsh BJ, Volkmann N, McIntosh JR, Howell KE (2004) Direct continuities between cisternae at different levels of the Golgi complex in glucose-stimulated mouse islet beta cells. Proc Natl Acad Sci USA 101(15):5565–5570
67. Martin S, Parton RG (2006) Lipid droplets: a unified view of a dynamic organelle. Nat Rev Mol Cell Biol 7(5):373–378
68. McMahon HT, Boucrot E (2011) Molecular mechanism and physiological functions of clathrin-mediated endocytosis. Nat Rev Mol Cell Biol 12(8):517–533
69. McMahon HT, Gallop JL (2005) Membrane curvature and mechanisms of dynamic cell membrane remodelling. Nature 438(7068):590–596
70. McMahon HT, Mills IG (2004) COP and clathrin-coated vesicle budding: different pathways, common approaches. Curr Opin Cell Biol 16(4):379–391
71. McMahon HT, Kozlov MM, Martens S (2010) Membrane curvature in synaptic vesicle fusion and beyond. Cell 140(5):601–605
72. Morris CE, Homann U (2001) Cell surface area regulation and membrane tension. J Membr Biol 179(2):79–102
73. Noguchi H (2016) Membrane remodeling from n-bar domain interactions: insights from multi-scale simulation. Sci Rep 6:20935
74. Peter BJ, Kent HM, Mills IG, Vallis Y, Butler PJG, Evans PR, McMahon HT (2004) BAR domains as sensors of membrane curvature: the amphiphysin bar structure. Science 303(5657):495–499
75. Polishchuk RS, Capestrano M, Polishchuk EV (2009) Shaping tubular carriers for intracellular membrane transport. FEBS Lett 583(23):3847–3856
76. Powers TR, Huber G, Goldstein RE (2002) Fluid-membrane tethers: minimal surfaces and elastic boundary layers. Phys Rev E 65(4):041901
77. Ramakrishnan N, Sunil Kumar PB, Ipsen JH (2013) Membrane-mediated aggregation of curvature-inducing nematogens and membrane tubulation. Biophys J 104(5):1018–1028
78. Raucher D, Sheetz MP (1999) Characteristics of a membrane reservoir buffering membrane tension. Biophys J 77(4):1992–2002
79. Raucher D, Sheetz MP (1999) Membrane expansion increases endocytosis rate during mitosis. J Cell Biol 144(3):497–506

80. Rink J, Ghigo E, Kalaidzidis Y, Zerial M (2005) Rab conversion as a mechanism of progression from early to late endosomes. Cell 122(5):735–749
81. Risselada HJ, Grubmüller H (2012) How snare molecules mediate membrane fusion: recent insights from molecular simulations. Curr Opin Struct Biol 22(2):187–196
82. Risselada HJ, Kutzner C, Grubmüller H (2011) Caught in the act: visualization of snare-mediated fusion events in molecular detail. ChemBioChem 12(7):1049–1055
83. Roux A, Cappello G, Cartaud J, Prost J, Goud B, Bassereau P (2002) A minimal system allowing tubulation with molecular motors pulling on giant liposomes. Proc Natl Acad Sci 99(8):5394–5399
84. Roux A, Koster G, Lenz M, Sorre B, Manneville J-B, Nassoy P, Bassereau P (2010) Membrane curvature controls dynamin polymerization. Proc Natl Acad Sci 107(9):4141–4146
85. Safran SA (1994) Statistical thermodynamics of surfaces, interfaces, and membranes. Addison-Wesley, Reading
86. Saleem M, Morlot S, Hohendahl A, Manzi J, Lenz M, Roux A (2015) A balance between membrane elasticity and polymerization energy sets the shape of spherical clathrin coats. Nat Commun 6(6249)
87. Schick M (2011) Membrane fusion: the emergence of a new paradigm. J Stat Phys 142(6):1317–1323
88. Sciaky N, Presley J, Smith C, Zaal KJM, Cole N, Moreira JE, Terasaki M, Siggia E, Lippincott-Schwartz J (1997) Golgi tubule traffic and the effects of Brefeldin A visualized in living cells. J Cell Biol 139(5):1137–1155
89. Seifert U (1997) Configurations of fluid membranes and vesicles. Adv Phys 46(1):13–137
90. Seifert U, Berndl K, Lipowsky R (1991) Shape transformations of vesicles: phase diagram for spontaneous-curvature and bilayer-coupling models. Phys Rev A 44(2):1182
91. Sens P, Turner MS (2006) Budded membrane microdomains as tension regulators. Phys Rev E 73:031918
92. Shaklee PM, Idema T, Koster G, Storm C, Schmidt T, Dogterom M (2008) Bidirectional membrane tube dynamics driven by nonprocessive motors. Proc Natl Acad Sci 105(23):7993–7997
93. Shen H, Pirruccello M, De Camilli P (2012) Snapshot: membrane curvature sensors and generators. Cell 150(6):1300–1300
94. Shillcock JC, Lipowsky R (2005) Tension-induced fusion of bilayer membranes and vesicles. Nat Mater 4(3):225–228
95. Sinha B, Köster D, Ruez R, Gonnord P, Bastiani M, Abankwa D, Stan RV, Butler-Browne G, Vedie B, Johannes L et al (2011) Cells respond to mechanical stress by rapid disassembly of caveolae. Cell 144(3):402–413
96. Smirnova YG, Marrink S-J, Lipowsky R, Knecht V (2010) Solvent-exposed tails as prestalk transition states for membrane fusion at low hydration. J Am Chem Soc 132(19):6710–6718
97. Solon J, Pécréaux J, Girard P, Fauré M-C, Prost J, Bassereau P (2006) Negative tension induced by lipid uptake. Phys Rev Lett 97(9):098103
98. Sorre B, Callan-Jones A, Manzi J, Goud B, Prost J, Bassereau P, Roux A (2012) Nature of curvature coupling of amphiphysin with membranes depends on its bound density. Proc Natl Acad Sci 109(1):173–178
99. Stachowiak JC, Hayden CC, Sasaki DY (2010) Steric confinement of proteins on lipid membranes can drive curvature and tubulation. Proc Natl Acad Sci 107(17):7781–7786
100. Stachowiak JC, Schmid EM, Ryan CJ, Ann HS, Sasaki DY, Sherman MB, Geissler PL, Fletcher DA, Hayden CC (2012) Membrane bending by protein–protein crowding. Nat Cell Biol 14(9):944–949
101. Stachowiak JC, Brodsky FM, Miller EA (2013) A cost-benefit analysis of the physical mechanisms of membrane curvature. Nat Cell Biol 15(9):1019–1027
102. Stagg SM, LaPointe P, Razvi A, Gürkan C, Potter CS, Carragher B, Balch WE (2008) Structural basis for cargo regulation of COPII coat assembly. Cell 134(3):474–484

103. Staykova M, Holmes DP, Read C, Stone HA (2011) Mechanics of surface area regulation in cells examined with confined lipid membranes. Proc Natl Acad Sci 108(22):9084–9088

104. Stevens MJ, Hoh JH, Woolf TB (2003) Insights into the molecular mechanism of membrane fusion from simulation: evidence for the association of splayed tails. Phys Rev Lett 91(18):188102

105. Takei K, Slepnev VI, Haucke V, De Camilli P (1999) Functional partnership between amphiphysin and dynamin in clathrin-mediated endocytosis. Nat Cell Biol 1(1):33–39

106. Takizawa PA, Yucel JK, Veit B, John Faulkner D, Deerinck T, Soto G, Ellisman M, Malhotra V (1993) Complete vesiculation of Golgi membranes and inhibition of protein transport by a novel sea sponge metabolite, ilimaquinone. Cell 73(6):1079–1090

107. Thiam AR, Pincet F (2015) The energy of COPI for budding membranes. PLoS One 10(7):e0133757

108. Thiam AR, Antonny B, Wang J, Delacotte J, Wilfling F, Walther TC, Beck R, Rothman JE, Pincet F (2013) Copi buds 60-nm lipid droplets from reconstituted water–phospholipid–triacylglyceride interfaces, suggesting a tension clamp function. Proc Natl Acad Sci 110(33):13244–13249

109. Thiam AR, Farese RV Jr, Walther TC (2013) The biophysics and cell biology of lipid droplets. Nat Rev Mol Cell Biol 14(12):775–786

110. Trucco A, Polishchuk RS, Martella O, Di Pentima A, Fusella A, Di Giandomenico D, San Pietro E, Beznoussenko GV, Polishchuk EV, Baldassarre M et al (2004) Secretory traffic triggers the formation of tubular continuities across golgi sub-compartments. Nat Cell Biol 6(11):1071–1081

111. Tsafrir I, Sagi D, Arzi T, Guedeau-Boudeville M-A, Frette V, Kandel D, Stavans J (2001) Pearling instabilities of membrane tubes with anchored polymers. Phys Rev Lett 86(6):1138

112. Tsafrir I, Caspi Y, Guedeau-Boudeville M-A, Arzi T, Stavans J (2003) Budding and tubulation in highly oblate vesicles by anchored amphiphilic molecules. Phys Rev Lett 91(13):138102

113. Upadhyaya A, Sheetz MP (2004) Tension in tubulovesicular networks of golgi and endoplasmic reticulum membranes. Biophys J 86(5):2923–2928

114. Vale RD, Hotani H (1988) Formation of membrane networks in vitro by Kinesin-driven microtubule movement. J Cell Biol 107(6):2233–2241

115. Walani N, Torres J, Agrawal A (2014) Anisotropic spontaneous curvatures in lipid membranes. Phys Rev E 89(6):062715

116. Walani N, Torres J, Agrawal A (2015) Endocytic proteins drive vesicle growth via instability in high membrane tension environment. Proc Natl Acad Sci 112(12):E1423–E1432

117. Waterman-Storer CM, Salmon ED (1998) Endoplasmic reticulum membrane tubules are distributed by microtubules in living cells using three distinct mechanisms. Curr Biol 8(14):798–807

118. Weber T, Zemelman BV, McNew JA, Westermann B, Gmachl M, Parlati F, Söllner TH, Rothman JE (1998) SNAREpins: minimal machinery for membrane fusion. Cell 92(6):759–772

119. Wilfling F, Thiam AR, Olarte M-J, Wang J, Beck R, Gould TJ, Allgeyer ES, Pincet F, Bewersdorf J, Farese RV et al (2014) Arf1/COPI machinery acts directly on lipid droplets and enables their connection to the ER for protein targeting. Elife 3:e01607

120. Yamada A, Mamane A, Lee-Tin-Wah J, Di Cicco A, Prévost C, Lévy D, Joanny J-F, Coudrier E, Bassereau P (2014) Catch-bond behaviour facilitates membrane tubulation by non-processive myosin 1b. Nat Commun 5:3624

121. Yang J-S, Valente C, Polishchuk RS, Turacchio G, Layre E, Moody DB, Leslie CC, Gelb MH, Brown WJ, Corda D et al (2011) COPI acts in both vesicular and tubular transport. Nat Cell Biol 13(8):996–1003

122. Zanetti G, Pahuja KB, Studer S, Shim S, Schekman R (2012) COPII and the regulation of protein sorting in mammals. Nat Cell Biol 14(1):20–28

123. Zanetti G, Prinz S, Daum S, Meister A, Schekman R, Bacia K, Briggs JAG (2013) The structure of the COPII transport-vesicle coat assembled on membranes. Elife 2:e00951

124. Zhong-Can O-Y, Helfrich W (1989) Bending energy of vesicle membranes: General expressions for the first, second, and third variation of the shape energy and applications to spheres and cylinders. Phys Rev A 39(10):5280
125. Zimmerberg J, Kozlov MM (2006) How proteins produce cellular membrane curvature. Nat Rev Mol Cell Biol 7(1):9–19